Orthophosphate nanostructures in SiO_2–P_2O_5–CaO–Na_2O–MgO bioactive glasses

H. Aguiar [a,*], E.L. Solla [a], J. Serra [a], P. González [a], B. León [a], N. Almeida [b], S. Cachinho [b], E.J.C. Davim [b,c], R. Correia [b,c], J.M. Oliveira [c,d], M.H.V. Fernandes [b,c]

[a] *Applied Physics Department, University of Vigo, Lagoas-Marcosende 9, 36310 Vigo, Spain*
[b] *Ceramics and Glass Engineering Department, University of Aveiro, 3810-193 Aveiro, Portugal*
[c] *Centre for Research in Ceramics and Composite Materials, CICECO, University of Aveiro, 3810-193 Aveiro, Portugal*
[d] *High School of North-Aveiro, University of Aveiro, Edifício Rainha, 5° Andar, 3720-232 Oliveira de Azeméis, Portugal*

ARTICLE INFO

ABSTRACT

Vibrational spectroscopy, ^{29}Si and ^{31}P magic-angle spinning nuclear magnetic resonance spectroscopy and high resolution transmission electron microscopy were used to investigate structural aspects of SiO_2–P_2O_5–CaO–Na_2O–MgO glasses. The experimental results show that for the two compositions, $25.3SiO_2$–$10.9P_2O_5$–$32.6CaO$–$31.2MgO$ and $33.6SiO_2$–$6.40P_2O_5$–$19.0CaO$–$41.0MgO$, phosphorous is present in a nano-crystalline form with interplanar distances in the 0.21–0.26 nm range. The two glasses develop a surface CaP-rich layer and the presence of any intermediate silica-rich layer was not detected. It was suggested that the phosphate nano-regions may play a key role in the initial stages of the bioactive process, acting as nucleation sites for the calcium phosphate-rich layer.

* Corresponding author. Tel.: +34 986 812 216; fax: +34 986 812 201.
  E-mail address: haguiar@uvigo.es (H. Aguiar).

1. Introduction

Since the early 70s, Hench's research work has been pursued to design new bioactive glasses and improve the bioactive properties of melt-derived silicate glasses. This persistent investigation responds to the medical care demands, such as cranial repair, otolaryngological and dental implants, maxillofacial reconstructions, percutaneous access devices, periodontal pocket obliteration, alveolar ridge augmentations, etc. [1,2].

The bioactive behavior of glasses is identified as their ability to react chemically with living tissues, forming with them mechanically strong and lasting bonds. These bone-bondings are attributed to the formation of an apatite-like layer on the glass surface, with composition and structure equivalent to the mineral phase of bone [3,4]. This property is related to the glass structure and composition. Particularly, silica-based glasses are structurally based in tetrahedral units $[SiO_4^{4-}]$ [5,6]. The central silicon atom with external electronic configuration $3s^2 3p^2$ assumes a tetrahedral hybrid state sp^3 and contributes one electron to each bond. Two cases can occur. In the first case, each oxygen atom with electronic configuration $1s^2 2s^2 2p_x^2 2p_y^1 2p_z^1$ uses their two unpaired electrons in σ covalent bonds with two neighbor silicon atoms ('bridging oxygen', BO). In the second case, each oxygen uses one unpaired electron in a σ covalent bond with the neighbor silicon atom, the other unpaired electron being available to ionically interact with alkaline or alkaline-earth metals, the so-called network modifiers (Na^+, K^+, Ca^{2+}, Mg^{2+}, etc.), forming 'non-bridging' oxygen (NBO) bonds. The presence of these cations results in a disruption of the continuity of the glassy network leading to an increment of the concentration of NBO groups. Since this concentration controls the dissolution rate of the silica through the formation of silanol groups at the glass surface, NBO's and the structure play a key role in the bioactive response of these glasses [1,7,8].

The network connectivity is conventionally expressed as Q^n units, where Q represents the tetrahedral structural unit and n the number of BO per tetrahedron. For silicon–oxygen networks, n varies between 0 and 4, where Q^0 represents orthosilicates (SiO_4^{4-}), Q^4 is pure SiO_2 and Q^3, Q^2 and Q^1 represent intermediate silicate structures. Modifier concentrations are thus needed to electronically stabilize structures Q^0–Q^3, the reason for which these structural units possess Si–O–NBO bonds. For P compounds, Q^0 represents orthophosphates (PO_4^{3-}), Q^3 a pure P_2O_5 structure corresponding to the absence of network modifiers, Q^2 (metaphosphate) and Q^1 (pyrophosphate) are intermediate structures [9].

The purpose of this investigation is to study the influence of the structure on the *in vitro* bioactive behavior in acellular medium of SiO_2–P_2O_5–CaO–Na_2O–MgO glasses, through different analytical characterization techniques, including Fourier-transform infrared (FTIR) and Raman spectroscopies (sensitive methods for detecting local changes in the network symmetry), and ^{31}P magic angle spinning nuclear magnetic resonance (^{31}P MAS-NMR) spectroscopy for disclosing the bonding structure of phosphorous. Complementary techniques were also used, namely X-ray diffraction (XRD) and high resolution transmission electron microscopy (HRTEM) with electron diffraction.

2. Materials and methods

Four different melt-derived glasses (MDG's) with compositions depicted in Table 1 were studied in this work. Both MDG25 and MDG33 are glasses with high MgO content and have the same CaO/P_2O_5 and SiO_2/MgO ratio (∼3 and 0.8, respectively). Previous work has shown that similar glasses induce the apatite precipitation in SBF [10,11] despite the high MgO content and the low SiO_2 content. Aiming to understand the influence of glass structure on their bioactive behavior, two other compositions were used as reference materials, a phosphate-free glass (MDG60) and a silica-free glass (MDGP).

All glasses were prepared by mixing analytical grade $Ca(H_2PO_4)_2$ and Na_2CO_3 (Fluka), $CaCO_3$, MgO and SiO_2 precipitated (BDH) with ethanol during 45 min and drying at 70 °C for 24 h. In order to produce a homogeneous glass, a double melting procedure was adopted. Batches of 80 g were melted in a platinum crucible, in air, at 1500 °C for 1 h, and poured into water in order to produce a glass frit. The frit was dried and remelted at 1500 °C for 2 h and poured onto a glass mould. The obtained block was annealed at 730 °C for 30 min, in air, and slowly cooled to room temperature. A portion of this block glass was crushed and reduced to powder, with particle size below 33 μm, for analysis. The remaining glass was cut in order to obtain cylindrical samples with

Table 1
Nominal compositions of studied and reference glasses

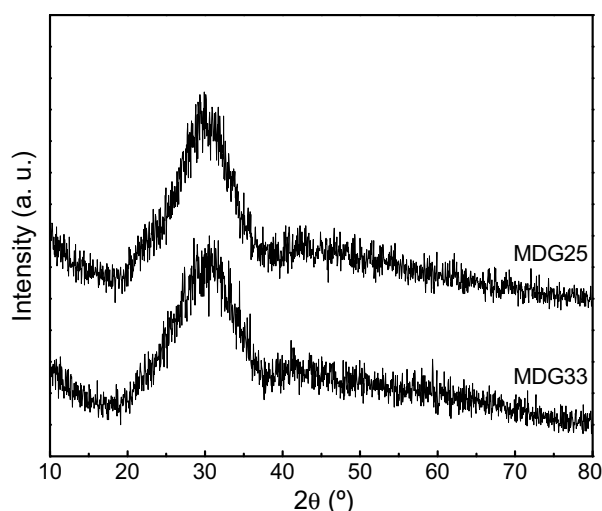| Oxide		Sample			
		MDG25	MDG33	MDG60	MDGP
(mol%)	SiO_2	25.3	33.6	60.0	–
	CaO	32.6	19.0	–	42.3
	P_2O_5	10.9	6.40	–	42.3
	MgO	31.2	41.0	35.0	15.4
	Na_2O	–	–	5.00	–

Fig. 1. XRD patterns of MGD25 and MDG33 samples.

20 mm in diameter and 2 mm thick. These glass discs were polished with sandpapers of different granulometries.

A portion of crushed glasses was taken for powder X-ray diffraction (XRD) using $CuK\alpha$ radiation. The Fourier-transform Raman spectrometer used a 2 W Nd:YAG laser ($\lambda = 1,06 \mu m$) (Bruker RFS100). The FTIR spectrometer operated in the mid-infrared range from 550 to 5000 cm^{-1} in reflection mode (Bruker RFS128). HRTEM was performed on a JEOL JEM-2010F, with a potential acceleration of 200 kV. ^{31}P MAS-NMR spectra were recorded on a BRUKER AVANCE spectrometer operating at 161.976 MHz, using 3.7 μs pulses and the chemical shift was quoted in ppm from 85% H_3PO_4 solution. The precision of the isotropic peak positions is about ±0.1 ppm.

In vitro assays of bioactivity were performed by soaking the material in simulated body fluid (SBF), an acellular aqueous solution with inorganic ion composition almost equal to human plasma, proposed by Kokubo et al. [4,12]. For this purpose, a surface area to volume ratio (SA/V of SBF solution) equal to 0.5 was used. After 72 h at 37 °C, the samples were gently rinsed with water, dried and analysed by scanning electron microscopy (Philips XL30) equipped with energy dispersive spectroscopy (SEM/EDS). The thickness of the layers that grew as a consequence of the bioactive process was measured on the SEM images. In order to estimate the uncertainty Δx of the SEM data, the systematic (Δx_s) and the random errors (Δx_r) were taken into account. This last error component was determined by measuring the thickness x_i on five different sites for the same layer, and then the average and the standard deviation were calculated. The systematic error corresponds to SEM resolution.

3. Results

3.1. Structural characterization

Fig. 1 shows X-ray diffractographs of MDG25 and MDG33, where no discernible peaks resulting from lattice periodicity are observed. This confirms that these glasses are amorphous at the discrimination level of the method.

Fig. 2(A) shows the typical Raman spectra of the investigated glasses, together with the reference phosphate glass. This figure reveals the presence of the main optical modes of the Si–O–Si groups as follows: (i) asymmetric stretching at 1000–1200 cm^{-1}, (ii) rocking at 560–660 cm^{-1}, and (iii) non-bridging silicon–oxygen bond (Si–O–NBO) stretching at 900–970 cm^{-1} [13–16]. This last Raman line cannot be assigned to phosphate groups because, as shown in Fig. 2(A), the experimental Raman analysis of MDGP (42.3 mol% P_2O_5) shows the main features located at 704, 1035 and 1173 cm^{-1}.

Fig. 2(B) shows the FTIR spectra of the samples, where the main vibration modes [17,18] can be identified: (i) Si–O–Si stretching at 1000–1200 cm^{-1}, (ii) Si–O–NBO stretching at 890–975 cm^{-1}, (iii) Si–O–Si bending near 750 cm^{-1}, and (iv) PO_4^{3-} antisymmetric bending at 570–600 cm^{-1}, associated with phosphorous in a crystal-like environment [19].

In order to clarify the contribution of phosphate groups to the glass structure, HRTEM analyses have been carried out. Fig. 3(a) shows the typical electron contrast of amorphous materials. By selecting an area of interest (b) and applying Fourier transform (FT), a diffuse diffraction pattern is obtained (c), characteristic of the amorphous material.

Nevertheless, one can observe pairs of bright dots, diametrically located, corresponding to repetitive frequencies. After filtering the image, a characteristic diffraction pattern of a monocrystalline structure is found (d) [20]. Inverting the FT, a reconstructed image of a nanocrystalline area (e), with interplanar distance of 0.22 ± 0.03 nm, is obtained. Repeating this procedure for other
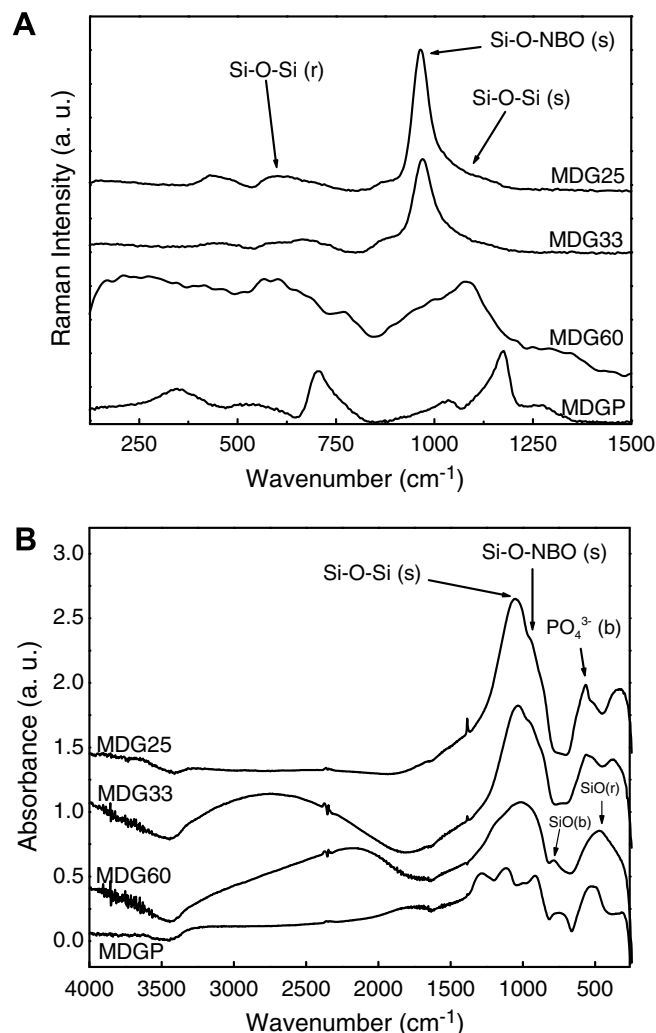
Fig. 2. Raman (A) and FTIR (B) spectra of MDG25, MDG33, MDG60 and MDGP samples.

interest areas of MDG25 and MDG33, interplanar distances in the 0.21–0.26 (±0.03) nm range, characteristic of phosphate networks, can be found [21].

Fig. 4 shows the HRTEM image of MDG60 glass. The electron micrograph shows the typical contrast of an amorphous material. Unlike the results obtained for MDG25 and MDG33 samples, the Fourier transform from the digitalized HRTEM image, Fig. 4(b), shows a broad diffused scattering and rings at low angles, indicative of an amorphous nature of MDG60 at the ultrastructural scale. These observations are in agreement with FTIR results.

With the purpose of corroborating the previous findings for MDG25 and MDG33 glasses, ^{31}P MAS-NMR studies were carried out (Fig. 5). As described in literature [22,23], we can identify single Q^0 bands at 1.87 ± 0.1 ppm and 1.18 ± 0.1 ppm in MDG25 and MDG33 spectra, respectively.

3.2. Bioactivity study

As proposed by Hench et al. [1,3], the bioactive mechanism in inorganic environment can be summarized in five steps: (i) rapid exchange of alkali or alkali-earth ions with H^+ or H_3O^+ from solution; (ii) loss of soluble silica in the form of $Si(OH)_4$ to the solution; (iii) condensation and repolymerization of SiO_2-rich layer on the surface depleted in alkalis and alkaline-earth cations; (iv) migration of Ca_2^+ and PO_4^{3-} groups to the surface through the SiO_2-rich

layer forming a CaO–P_2O_5-rich film on top of the SiO_2-rich layer, followed by the growth of the amorphous CaO–P_2O_5-rich film by incorporation of soluble calcium and phosphorous from solution; v) crystallization of the amorphous CaO–P_2O_5 film by incorporation
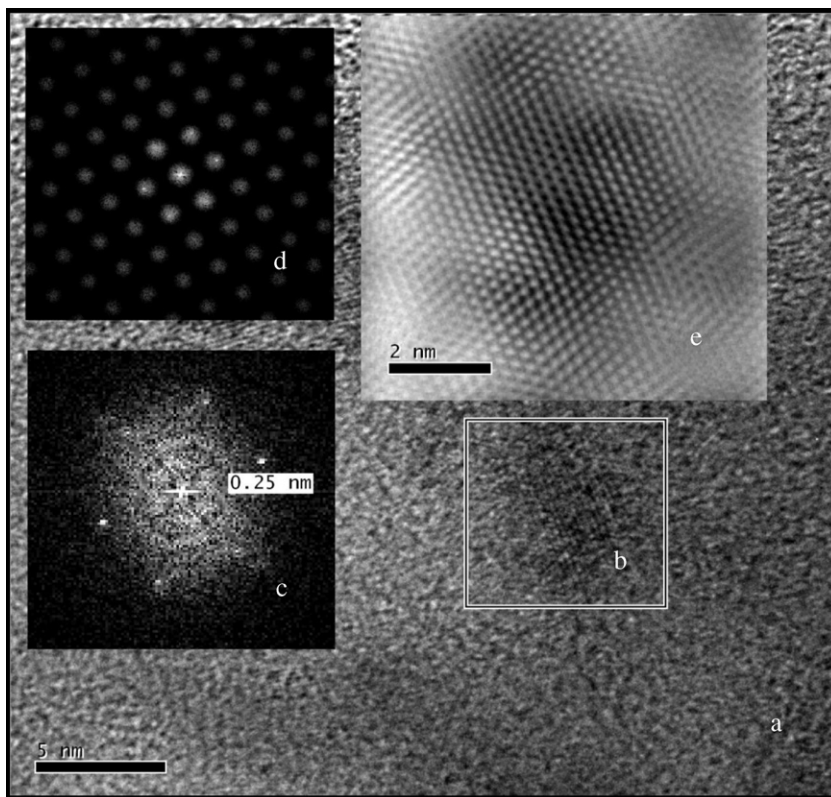

Fig. 3. HRTEM images of MDG33 glass: (a) amorphous matrix; (b) area of interest; (c) FT diffuse diffraction pattern with bright dots; (d) filtered FT; (e) reconstructed nanocrystalline areas.
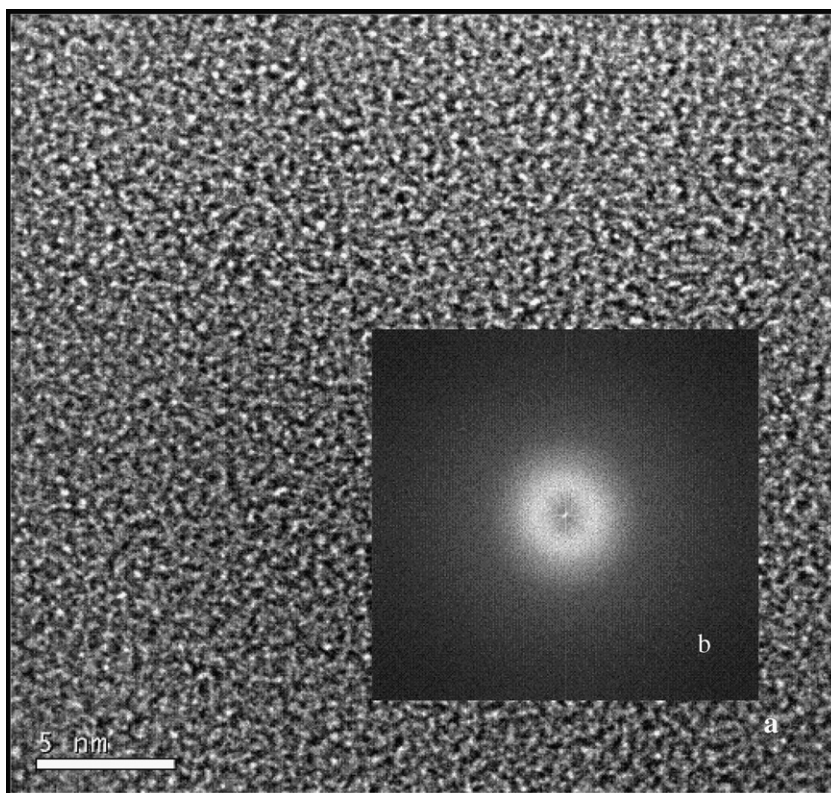

Fig. 4. HRTEM images of MDG60: (a) fully amorphous glass matrix; (b) fully diffuse diffraction pattern.
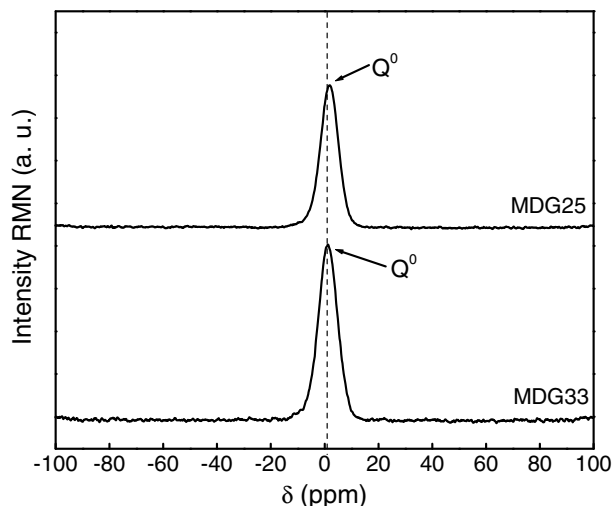
Fig. 5. ^{31}P MAS-NMR spectra of MDG25 and MDG33 samples.

of OH–, CO_3^{2-}, or F$^-$ anions from solution to form a mixed hydroxy–carbonate–fluorapatite layer.

In order to assess the bioactive response, *in vitro* tests were carried out, soaking MDG25, MDG33 and MDG60 glasses in SBF. The sample MDG60 does not show bioactive response. Fig. 6 shows the typical SEM micrograph of MDG25 glass taken after immersion during 72 h at 37 °C. The formation of two differentiated calcium phosphate layers (CaP and CaP + Si_xO_y) can be distinguished on MDG25 surfaces, confirmed by representative EDS analyses. The sample MDG33 shows the same behavior.

4. Discussion

It is commonly known that the incorporation of modifier elements into glass network promotes structural changes, detectable

by vibrational spectroscopy [7,16,18]. A deep analysis of Raman spectra (Fig. 2) allows noticing that the relative intensity and the position of Raman lines change with the glass composition, which varies with the incorporation of the modifier elements in the SiO_2 matrix. This fact makes evident the distortion that the glass network suffers as a result of the incorporation of the alkali and alkali-earth elements [16].

On the other hand, the appearance of an incipient PO_4^{3-} doublet in the FTIR spectra (Fig. 2(B)) suggests that phosphate groups can be present in a crystal-like environment [19]. These results confirm some optical modes identified by Raman spectroscopy and reveal the FTIR sensitivity for detecting phosphate vibrational bands, which makes evident the complementation of both spectroscopic techniques. All these results obtained by IR and Raman analyses for MDG25 and MDG33 samples are in perfect agreement with previous works [7,16,18,24], except for the observed PO_4^{3-} antisymmetric bending mode, which reveals a greater IR activity of phosphate groups.

Basing on HRTEM and RMN analyses, it can be assumed that phosphate groups form isolated orthophosphate nanocrystalline islands in the amorphous matrix of MDG25 and MDG33 samples. Furthermore, a small displacement of Q^0 bands ($\Delta\delta = 0.7 \pm 0.1$ ppm) observed in RMN spectra (Fig. 5) seems consistent with compositional differences in both glasses (Table 1), leading to a distinctly disordered chemical environment [23]. Besides, the presence of single bands with equal line width in both glasses ($\Delta_{1/2} = 7.9 \pm 0.1$ ppm) is in agreement with the filtered FT diffraction pattern (Fig. 3(c)), associated with single crystals.

Measurements of the thickness of the layers identified through SEM/EDS were carried out (Fig. 7) with the purpose of deepening the quantitative evolution of the bioactive response of MDG25 and MDG33 samples. A good agreement with the theoretical predictions, in which glasses with lower modifier content are less reactive in physiological environment, is observed [1,3,7]. In accordance with a small difference in the respective modifier concentrations, MDG25 is slightly more bioactive than MDG33 glass. Moreover, a deeper analysis of MDG25 and MDG33 SEM images
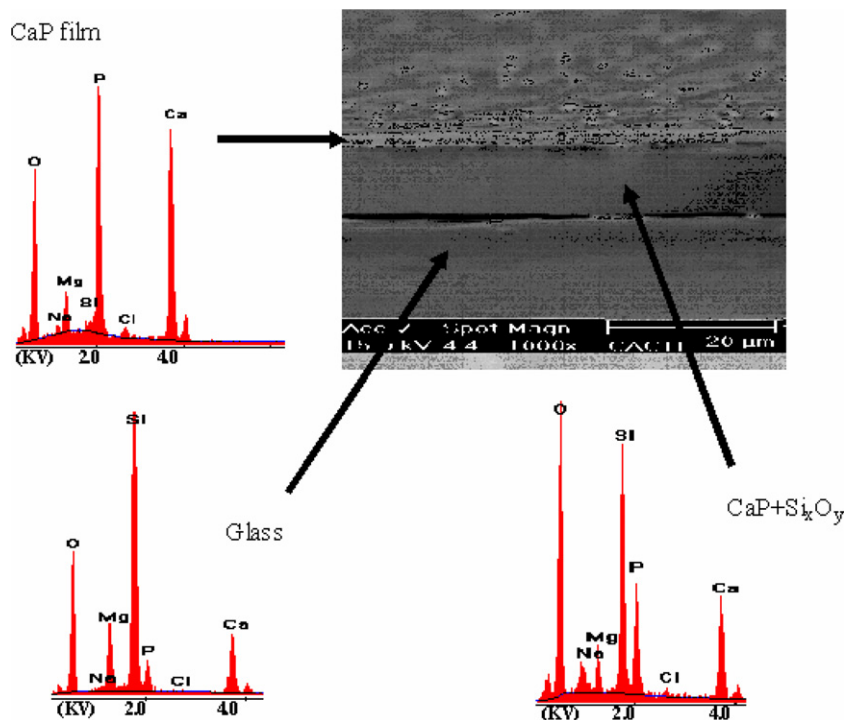

Fig. 6. Typical SEM micrograph of bioactive glass (MDG25) and EDS analyses after soaking during 72 h in SBF. No SiO_2-rich layer presence.
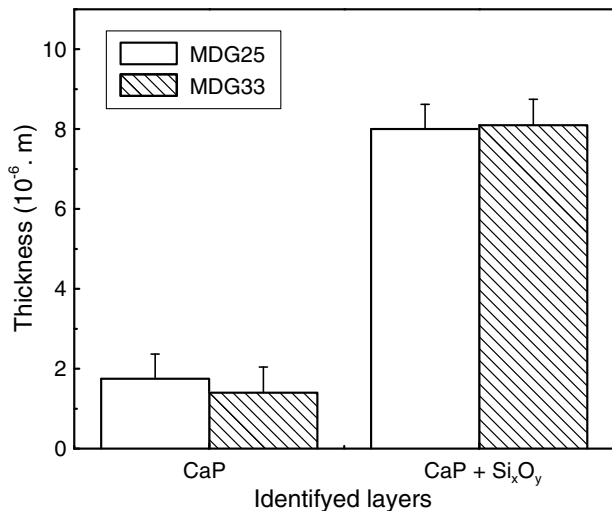
Fig. 7. CaP and CaP + Si_xO_y thickness of surface layers.

allows realizing that there were no signs of the presence of an intermediate silica-rich layer in both bioactive glasses (Fig. 6), which is confirmed by the corresponding EDS spectra. This behavior has been reported in other materials [1] and suggests the precipitation of an apatite layer on the glass surface, however, the formation of a SiO_2-rich layer is absent. The bioactive mechanism of the glass can be discussed following the well-known models reported in literature [1,25]. In this work, the bioactive behavior of these glasses cannot be compared with those of glass-ceramics in SBF, namely on the nucleation and the growth of apatite layers, since glasses and crystallized glasses (or glass-ceramics) are structurally very different and, thus, different mechanisms of apatite precipitation in SBF are found, as previously reported [26–28]. As proposed by Andersson et al. [25], CaP and silica-rich layers could form at the same time through a competitive process. On the other hand, the higher concentration of modifiers in MDG25 and MDG33 glass leads to a higher depolymerization degree of the structure and a higher concentration of the Si–O–NBO groups. These functional groups control the dissolution of the silica through the formation of silanol groups at the glass surface (stage ii) [1,5,16]. In addition, the presence of orthophosphate groups in isolated crystalline nano-regions promotes a microstructure with areas where the chemical connection of the glass structure is weaker. These areas can be the preferential sites for the chemical attack during the SBF immersion. It has been proposed that these peculiar properties favor an increase in the rate of some stages during the bioactive process. The ionic exchange and the silica dissolution (stage i and ii, respectively) must take place very quickly, as suggested by the EDS analysis. Moreover, it appears that there is no time for the condensation and repolymerization of SiO_2-rich layer (stage iii) before the precipitation of the CaP-rich film (stage iv). Thus, in general, these glasses may follow Hench's mechanism, but with particular characteristics due to kinetic factors.

5. Conclusions

Bioactive SiO_2–P_2O_5–CaO–Na_2O–MgO glasses obtained by melting and casting present an overall amorphous structure with the orthophosphate groups in isolated nanocrystal-like regions. As a consequence, phosphorous does not act as a network former. The presence of the CaP-rich film and the absence of a silica-rich layer during mineralization in SBF suggest that the phosphate nano-regions may play a key role in the initial stages of the bioactive process, acting as nucleation sites for a calcium phosphate-rich film.

References

[1] L.L. Hench, Ö. Andersson, An Introduction to Bioceramics, World Scientific, Singapore, 1993. p. 41.
[2] M. Vallet-Regí, J. Chem. Soc., Dalton Trans. (2001) 97.
[3] L.L.Hench, Hench, R.J.Splinter, Splinter, W.C.Allen, Allen, J. Biomed. Mater. Res. Symp. 2 (1971) 117.
[4] T. Kokubo, Acta Mater. 2519–2527 (1998) 46.
[5] F.L. Galeener, Phys. Rev. B 19 (1979) 4292.
[6] A.L. Companion, in: Enlaces Químicos, Editorial Reverté S.A., Barcelona, 1980.
[7] J. Serra, P. González, S. Liste, S. Chiussi, B. León, M. Pérez-Amor, H.O. Ylänen, M. Hupa, J. Mater. Sci. Med. 1221–1225 (2002) 13.
[8] P.H. Gaskell, in: J. Zarzycki (Ed.), Glass and Amorphous Materials, Materials Science and Technology, vol. 9, VCH, Weinheim, 1991, p. 175.
[9] G. Walter, J. Vogel, U. Hoppe, P. Hartmann, J. Non-Cryst. Solids 210–222 (2003) 320.
[10] J.M. Oliveira, R.N. Correia, M.H.V. Fernandes, Biomaterials 23 (2) (2002) 371.
[11] D. Pereira, S. Cachinho, M.C. Ferro, M.H.V. Fernandes, J. Eur. Ceram. Soc. 24 (2004) 3693.
[12] T. Kokubo, H. Kushitani, C. Ohtsuki, S. Sakka, T. Yamamuru, J. Mater. Sci. Med. 79–83 (1992) 3.
[13] A.E. Geissberger, F.L. Galeener, Phys. Rev. B 28 (1983) 3266.
[14] F. Gallener, G. Lucovsky, Phys. Rev. Lett. 37 (1976) 1474.
[15] W.A. Pliskin, J. Vac. Sci. Technol. 14 (1977) 1064.
[16] P. González, S. Serra, S. Liste, S. Chiussi, B. León, M. Pérez-Amor, J. Non-Cryst. Solids 92–99 (2003) 320.
[17] U. Posset, E. Löcklin, R. Thull, W. Kiefer, J. Biomed. Mater. Res. 40 (1998) 640.
[18] J. Serra, P. González, S. Liste, C. Serra, S. Chiussi, B. León, M. Pérez-Amor, H.O. Ylänen, M. Hupa, J. Non-Cryst. Solids 20–27 (2003) 322.
[19] J.C. Elliott, in: Structure and Chemistry of the Apatites and other Calcium Orthophosphates, Elsevier, Amsterdam, 1994, p. 59.
[20] D.B. Williams, C.B. Carter, in: Transmission Electron Microscopy, Plenum, New York, 1996.
[21] M. Vallet-Regí, A.J. Salinas, J.R. Castellanos, J.M. Calbet, Chem. Mater. 1874–1879 (2005) 17.
[22] M.W.G. Lockyer, D. Holland, R. Dupree, J. Non-Cryst. Solids 207–219 (1995) 188.
[23] J.J. Fitzgerald, in: J.J. Fitzgerald (Ed.), Solid-State NMR Spectroscopy of Inorganic Materials, Oxford University Press, South Dakota State University, 1999.
[24] J.P. Borrajo, S. Liste, J. Serra, P. González, S. Chiussi, B. León, M. Pérez-Amor, Key Eng. Mater. 284–286 (2005) 465.
[25] K.H. Karlsson, Glass Phys. Chem. 24 (3) (1998) 280.
[26] A.J. Salinas, J. Roman, M. Vallet-Regi, J.M. Oliveira, R.N. Correia, M.H.V. Fernandes, Biomaterials 21 (3) (2000) 251.
[27] J. Roman, A.J. Salinas, M. Vallet-Regi, J.M. Oliveira, R.N. Correia, M.H.V. Fernandes, Biomaterials 22 (14) (2001) 2013.
[28] C.M. Queiroz, J.R. Frade, M.H.V. Fernandes, Key Eng. Mater. 254–256 (2004) 155.